Journal of Physics: Condensed Matter

PAPER

# Weak localization in bilayer graphene with Li-intercalation/desorption

To cite this article: Y Endo *et al* 2018 *J. Phys.: Condens. Matter* **30** 305701

IOP Publishing Journal of Physics: Condensed Matter
J. Phys.: Condens. Matter **30** (2018) 305701 (7pp) https://doi.org/10.1088/1361-648X/aaccc4

# Weak localization in bilayer graphene with Li-intercalation/desorption

**Y Endo[1], S Ichinokura[1], R Akiyama[1], A Takayama[1], K Sugawara[2,3], K Nomura[3,4], T Takahashi[2,3,5] and S Hasegawa[1]**

[1] Department of Physics, The University of Tokyo, Tokyo 113-0033, Japan
[2] WPI Research Center, Advanced Institute for Materials Research, Tohoku University, Sendai 980-8577, Japan
[3] Center for Spintronics Research Network, Tohoku University, Sendai 980-8577, Japan
[4] Institute for Materials Research, Tohoku University, Sendai 980-8577, Japan
[5] Department of Physics, Tohoku University, Sendai 980-8578, Japan

E-mail: y.endo@surface.phys.s.u-tokyo.ac.jp

Received 4 April 2018, revised 11 June 2018
Accepted for publication 14 June 2018
Published 2 July 2018

**Abstract**

We performed *in-situ* electrical transport measurements for bilayer graphene grown on SiC(0 0 0 1) substrate, Li-intercalated bilayer graphene, and after that desorbing Li atoms by heating. Bilayer graphene after desorbing intercalated Li atoms showed a higher resistivity and different behavior in magnetoconductance compared to pristine bilayer graphene. We observed the weak localization of carriers at low temperatures in all the three samples and analyzed the experimental results with the extended Hikami–Larkin–Nagaoka equation to investigate the transport properties. The result shows that the magnetoconductance of pristine bilayer graphene is described by the AB stacking structure model and the phase breaking scattering is dominated by the electron–electron scattering. The intra-valley scattering occurs most frequently probably due to dopants in SiC substrate. However, in Li-desorbed graphene, the magnetoconductance can be described by neither AB nor AA-stacking model, suggesting the coexistence of domains with several different stacking structures.

Keywords: graphene, weak localization, quantum coherent transport, intercalation, atomic layer, Berry phase, stacking structure

S Supplementary material for this article is available online

(Some figures may appear in colour only in the online journal)

## 1. Introduction

Graphene, a single atomic sheet of graphite, has been a target of intensive studies because of the novel properties arising from the notable two-dimensional (2D) and massless nature of carriers therein [1–3]. The effects of quantum interference in 2D electron systems, such as weak localization (WL) and weak antilocalization (WAL), have been intensively studied because they provide rich information on the electronic transport property [4, 5]. In particular, exfoliated monolayer and bilayer graphene and monolayer graphene grown on SiC substrate have been used as a platform for observing such various novel phenomena [6–13]. Previous studies clarified a substantial contribution from the electron–electron interaction and WL to the resistivity and its sub-micrometer coherence lengths. The transport property of bilayer graphene grown on SiC substrate, however, has not been sufficiently investigated whereas it is abundant in novel phenomena such as 2D superconductivity [14, 15].

Graphite intercalation compounds (GICs) show various novel properties such as superconductivity and magnetism. GICs are widely used for technological application like an electrode of Li-ion battery and chemical catalysis [16]. Recently, graphene intercalation compounds, the thinnest limit of GICs, are attracting much attention as a platform for 2D superconductivity and electrochemical devices [14,

 

15]. Li-intercalated graphene has been actively investigated in these days for application to Li-ion nano-battery [17, 18]. However, the basic process of Li intercalation and de-intercalation is still unclear, in particular, in the relation to the electronic transport property.

In this paper, we report an *in situ* electrical transport measurement study of bilayer graphene grown on SiC substrate to investigate the change in the transport properties upon Li-intercalation and desorption (de-intercalation). We found that the temperature and magnetic-field dependences of the resistivity in bilayer graphene are well explained in terms of the WL effect. We observed that the conductivity was remarkably enhanced upon Li-intercalation, while it was drastically reduced upon desorption of Li to the value much lower than that of pristine bilayer graphene. The observed WL effect in Li-desorbed sample cannot be explained with the same model as used in pristine bilayer graphene, implying a significant structural change during the Li-intercalation/desorption process.

## 2. Experimental

Figures 1(a)–(c) show RHEED patterns of pristine, Li-intercalated and Li-desorbed bilayer graphene, respectively. Pristine bilayer graphene (called $S_1$ hereafter) was prepared on an *n*-type Si-rich 6*H*-SiC(0 0 0 1) substrate by direct heating up to 1550 °C under 1 atm argon atmosphere in an ultrahigh vacuum (UHV) chamber. By precisely controlling the heating temperature and the duration time, we succeeded in fabricating bilayer graphene [17]. The number of graphene sheets was confirmed by observing the band dispersions near *K* point in the Brillouin zone by angle-resolved photoemission spectroscopy (ARPES) [17]. After a short-time exposure to air, the bilayer graphene sample was transferred to another UHV system equipped with a reflection high-energy electron diffraction (RHEED) apparatus, Li evaporator, and a resistance measurement system [19]. As seen in figure 1(a), after heating up to 500 °C under UHV to remove contaminants adsorbed on the surface, the RHEED pattern from $S_1$ clearly exhibited the graphene's $1 \times 1$ and the buffer layer's $(6\sqrt{3} \times 6\sqrt{3})$R30° spots. Deposition of Li atoms was carried out using a Li dispenser (SAES Getters) at room temperature under UHV ($3 \times 10^{-10}$ Torr). The resultant sample ($S_2$) showed a RHEED pattern of $(\sqrt{3} \times \sqrt{3})$R30° characteristic of Li-intercalated bilayer graphene (figure 1(d)) [14, 17] with no trace of $(6\sqrt{3} \times \sqrt{3})$R30° spots. The third sample ($S_3$) was prepared by heating $S_2$ sample at 900 °C in UHV to desorb the Li atoms until the $(\sqrt{3} \times \sqrt{3})$R30° pattern disappeared and the $(6\sqrt{3} \times 6\sqrt{3})$R30° pattern from the buffer layer recovered as shown in figure 1(c).

The transport measurements were performed by the *in situ* four-point probe (4PP) technique in a UHV system (Unisoku USM-1300S) without exposing the samples to air [19]. The 4PP consists of four copper wires of 100 $\mu$m in diameter, aligned on a line with the probe spacing of ca. 200 $\mu$m. The sheet resistance $R_s$ was obtained by the 4PP dc current–voltage measurement by using the dual configuration method to avoid the data scattering due to the error in the probe spacing [19–22].

## 3. Results and discussion

Figure 2(a) shows the temperature dependence of conductance for $S_1$–$S_3$. The conductance of $S_2$ (Li-intercalated one) is ~3 times higher than that of $S_1$ (pristine), and it is remarked that $S_3$ (Li-desorbed one) exhibits lower conductance than $S_1$, although the RHEED pattern of $S_3$ looks similar to that of $S_1$. The increase in conductance from $S_1$ to $S_2$ is due to doping of electrons by intercalated Li atoms. As seen in figure 2(b), we performed the same experiment by using another sample, and then found a scattering in the conductance for $S_2$ from sample to sample, while the conductance of $S_1$ and $S_3$ was well reproducible. This scattering in conductance value in $S_2$ may be due to difference in the amount of Li atoms intercalated in and/or adsorbed on graphene. However, the carrier density of $S_2$ is at least ~16 times larger than that of $S_1$ estimated from the band dispersion by ARPES [17]. According to the result of low-energy electron microscopy (LEEM), Li-intercalation induces wrinkles/cracks and defects in graphene [23], which implies that the Li-intercalation process causes additional scattering centers for carriers.

We also found that the conductance of $S_3$ is lower than that of $S_1$. To reveal the origin of this difference, we compared the conductance of $S_1$ with that of $S_1$ after only heating at 900 °C without Li-intercalation/desorption. As a result, we found that there was little difference between the two samples (figure 1(c)), suggesting that the process of Li-intercalation and desorption should play a major role to induce the irreversible change in the conductance from $S_1$ to $S_3$.

Figure 2(d) shows the temperature dependence of conductance of $S_1$–$S_3$. When lowering the temperature from 30 K, the conductivity of $S_1$ at first shows a gradual increase till ~7 K and then rapidly decreases at low temperatures as seen in figure 2(d). This rapid decrease of conductance is a characteristic behavior of localization. In the case of $S_2$ and $S_3$, on the other hand, a decrease of conductance appears to start at a higher temperature at around 30 K although the reduction speed is not so rapid as $S_1$. This difference suggests that $S_2$ and $S_3$ have stronger localization than $S_1$.

Now we discuss in details the conductivity of pristine bilayer graphene ($S_1$) in relation to the WL and WAL effects [12, 13]. The WL occurs when an electron travels a closed path clockwise and anti-clockwise simultaneously to interfere constructively with itself, while the WAL is a result of destructive interference of these two time-reversal processes [24–26]. Whereas the electron is scattered elastically many times during these processes, the phase coherence of wave function is preserved within a finite distance called the phase breaking length $L_\phi$. Then, such phase coherence is broken by the inelastic scattering. As a result, the electron forms a standing wave around the closed path within $L_\phi$, leading to the decrease (increase) of the electrical conductance due to the WL (WAL). In the case of graphene, WL and WAL can be better explained with three characteristic lengths: the phase

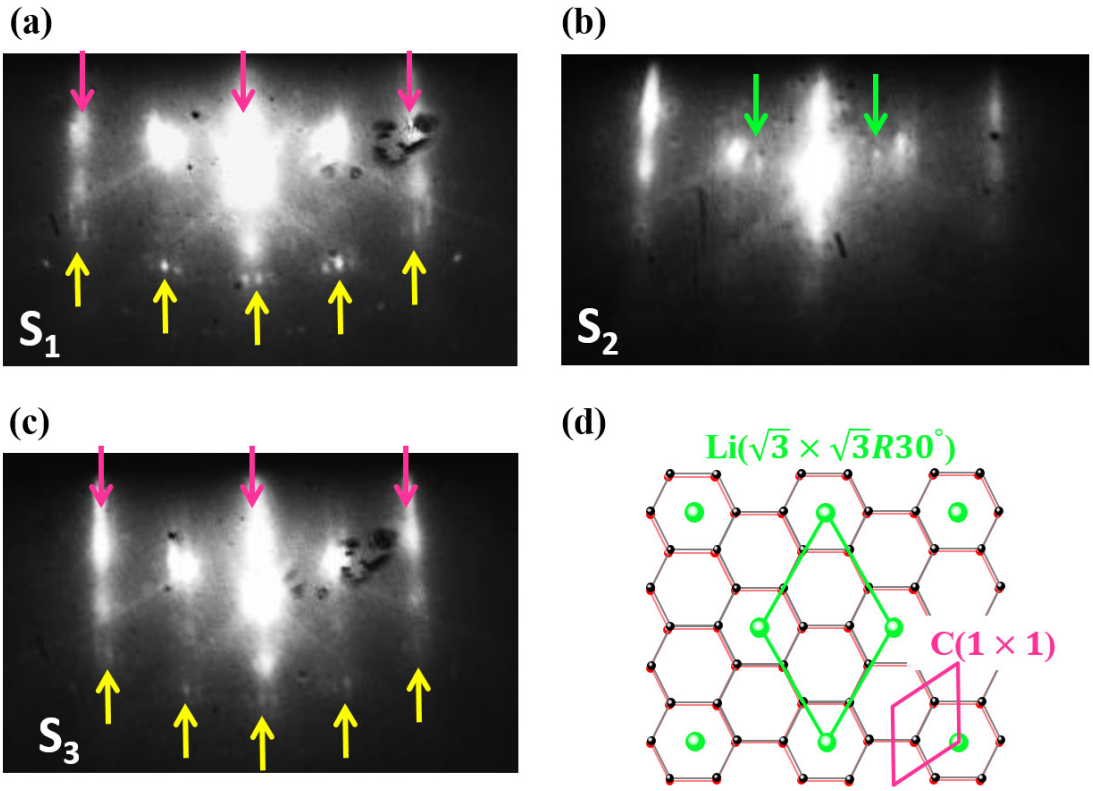


**Figure 1.** RHEED patterns of (a) pristine bilayer graphene grown on SiC(0 0 0 1) ($S_1$), (b) Li-intercalated bilayer graphene ($S_2$), and (c) bilayer graphene heated at 900 °C after Li-intercalation to desorb Li atoms ($S_3$). Pink, yellow and green arrows indicate the (1 × 1) pattern of graphene, the (6 $\sqrt{3}$ × 6 $\sqrt{3}$)R30° pattern of the buffer layer, and the ($\sqrt{3}$ × $\sqrt{3}$)R30° pattern of intercalated Li atoms, respectively. (d) Schematic view of atomic arrangement of Li-intercalated bilayer graphene in AA stacking. Green balls are Li atoms intercalated between graphene layers. Pink and green rhombuses are unit cells of graphene and Li intercalated graphene, respectively.

breaking length $L_\phi$, the inter-valley scattering length $L_i$, and the intra-valley scattering length $L_*$ as shown in figure 3(a). There are two kinds of well-defined stacking structures for bilayer graphene, which are called as AB stacking and AA stacking (figures 3(b) and (c)). Magnetic field dependence of conductivity in AB and AA stacking bilayer graphene is described by the extended Hikami–Larkin–Nagaoka (HLN) equation as equation (1) [9–11, 27, 28] and equation (2), respectively;

$$\Delta\sigma_{AB} = \sigma(B) - \sigma(0) = \frac{e^2}{\pi h}\left[F\left(\frac{B}{B_\phi}\right) - F\left(\frac{B}{B_\phi + 2B_i}\right) + 2F\left(\frac{B}{B_\phi + B_i + B_*}\right)\right], \quad (1)$$

$$\Delta\sigma_{AA} = \sigma(B) - \sigma(0) = \frac{2e^2}{\pi h}\left[F\left(\frac{B}{B_\phi}\right) - F\left(\frac{B}{B_\phi + 2B_i}\right) - 2F\left(\frac{B}{B_\phi + B_i + B_*}\right)\right]. \quad (2)$$

In both equations, the first and second terms describe the WL behavior and $F(x) \equiv \log x + \Psi\left(\frac{1}{2} + \frac{1}{x}\right)$, where $\Psi$ is a digamma function. $B_\phi$, $B_i$, and $B_*$ are defined as $B_{\phi,\ i,*} \equiv \hbar/(4eD\tau_{\phi,\ i,*}) = \hbar/\left(4eL^2_{\phi,\ i,*}\right)$, where $D$ is the diffusion coefficient and $\tau_{\phi,i,*}$ is the scattering time for the phase breaking scattering ($\tau_\phi$), the inter-valley scattering ($\tau_i$), and the intra-valley scattering ($\tau_*$), respectively. The factor 2 on the right-hand side in equation (2) comes from double Dirac cones in AA stacking bilayer graphene [29, 30]. Equation (1) has factor 1 because AB stacking bilayer graphene possesses a parabolic band. Namely, the factor depends on the number of channels. The third term in both equations (1) and (2) represents an opposite sign each other corresponding to the Berry phase. When the Berry phase is $2\pi$ for AB stacking bilayer graphene, the third term has a positive sign indicative of WL [9–11, 27, 28]. In bilayer graphene with AA stacking which has the linear band dispersion, the Berry phase is $\pi$, resulting in the negative sign in the third term related to WAL. Generally, the third term has much less contribution than the first and second terms in equations (1) and (2) because of the small intra-valley scattering length ($L_*$) [9].

Figure 3(d) shows the change in conductance $\Delta\sigma$ of $S_1$ upon applying the perpendicular magnetic field $B$. The conductance increases with increasing the magnetic field at all temperatures ($T$ = 1–15 K). This $B$ dependence is explained in terms of the time-reversal-symmetry breaking in WL, that is, the phase of electron is changed with increasing the magnetic field due to the Aharonov–Bohm effect, leading to breaking of the localization (constructive) interference. Black solid curves in figure 3(d) are the results of numerical fitting with equation (1). We find a good agreement, in particular, in the range of low magnetic field (below ~60 mT) between experiments

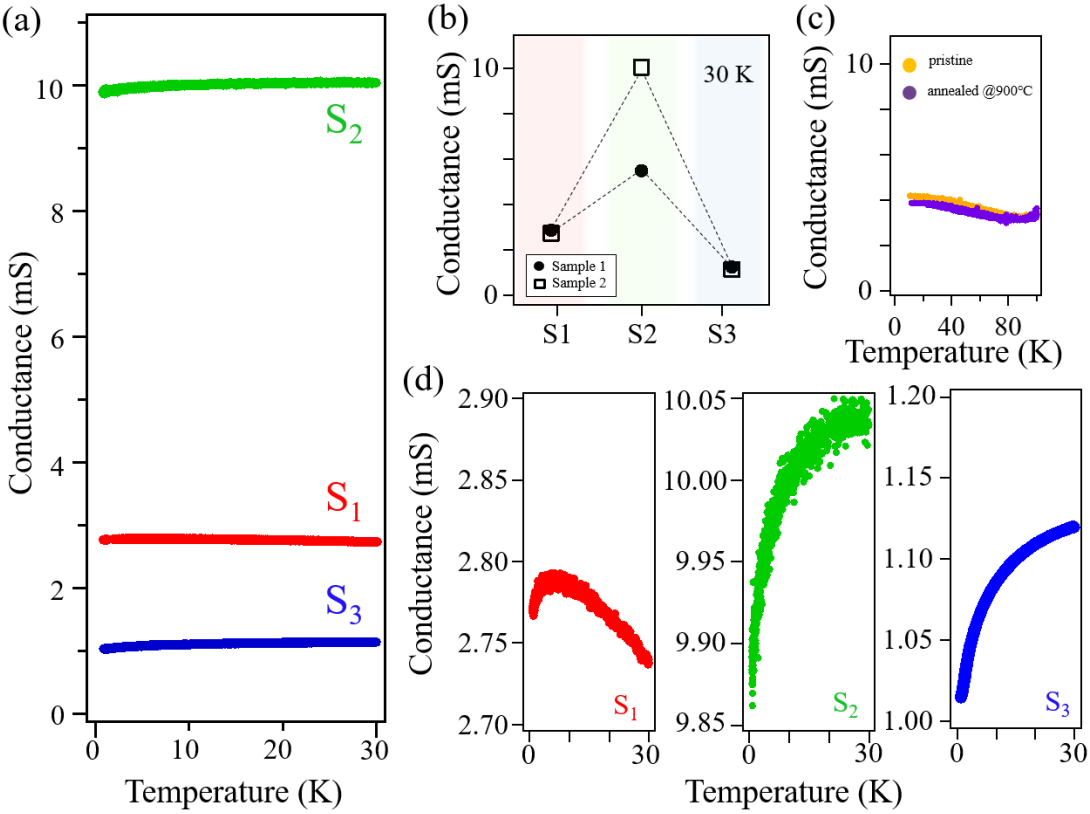


**Figure 2.** (a) Temperature dependences of conductance among $S_1$, $S_2$ and $S_3$. (b) Comparison of conductance at 30 K in $S_1$, $S_2$ and $S_3$ states between two independent samples. A scattering in conductance value is seen in $S_2$ state. (c) Comparison of temperature dependence of conductance between pristine ($S_1$) and that after just heating up to 900 °C without Li intercalation. (d) Conductance of $S_1$–$S_3$ at low temperatures in an expanded scale.

and fittings, which suggests the valid applicability of AB stacking model to pristine bilayer graphene ($S_1$). We have derived parameters $B_\phi$, $B_i$, and $B_*$, together with the corresponding scattering times $\tau_\phi$, $\tau_i$, and $\tau_*$, by fitting the curves, and summarize the results in table 1.

The temperature dependences of $L_{\phi,i,*}$ are plotted in figure 3(e). The $L_\phi$ depends on temperature $T$ as $L_\phi \propto T^{-P/2}$. When $P$ is close to 1 (2), the phase breaking is caused by the electron–electron interaction (the electron–phonon interaction) [31–33]. In $S_1$, the $L_\phi$ was fitted with $P = 0.83$, as seen in figure 3(e), indicating that the phase breaking is dominated by the electron–electron interaction in pristine bilayer graphene grown on SiC.

Figure 3(f) was derived by fitting curves in figure 3(d) using equation (2) with the AA stacking form. The $L_\phi$ was fitted with $P = 0.46$, which, however, is much smaller than the theoretical value (1 or 2). Thus, it is suggested that the AA stacking model is not suitable for pristine bilayer graphene ($S_1$), consistent with the theoretical calculation result that the AB stacking structure is energetically stable than AA stacking for bilayer graphene [34].

$S_2$ also shows the WL behavior as seen in the supplementary data (figure S1) (stacks.iop.org/JPhysCM/30/305701/mmedia), but the change of magnetoconductance is too small to fit accurately by using equation (1) or equation (2). This may be due to the carrier doping by intercalated Li [17], and thus we have performed a fitting to $S_2$ by the original HLN equation to obtain only the $L_\phi$. The fitting result shows that $L_\phi = 170 \pm 20$ nm at 1 K, which is relatively smaller than the value of pristine bilayer graphene ($L_\phi = 588 \pm 106$ nm). This difference suggests the increase of phase breaking scattering by Li-intercalation.

Figure 3(g) shows the change in conductance $\Delta\sigma$ of $S_3$ upon applying the surface-normal magnetic field $B$. The $B$ dependence can be also interpreted as breaking of the localization (constructive) interference. On the other hand, the $B$ range of increasing conductance is larger than that of $S_1$ by at least one order of magnitude, meaning the increase in population of scatterers. The $B$ dependence of $S_3$ was analyzed by equations (1) and (2). Each result is shown in figures 3(h) and (i), respectively. Theoretically, since the inter and intra-valley scatterings originate from the impurity/defect scattering, the $L_{i,*}$ should be temperature-independent. However, $L_i$ shows a non-negligible temperature dependence in both figures 3(h) and (i). Furthermore, the $L_\phi$ was fitted by $L_\phi \propto T^{-P/2}$ as the solid curves in figures 3(h) and (i), and the obtained $P$ values are 0.27 and 0.22, respectively. These values are too small compared with the theoretical one (1 or 2). All these results indicate that $S_3$ cannot be described by either pure AB or AA stacking model. This implies that the Li-intercalation/desorption process induces a change in the stacking structure from the AB stacking in pristine bilayer graphene to a mixed domains of different stacking structures including twisted stacking structure [35].

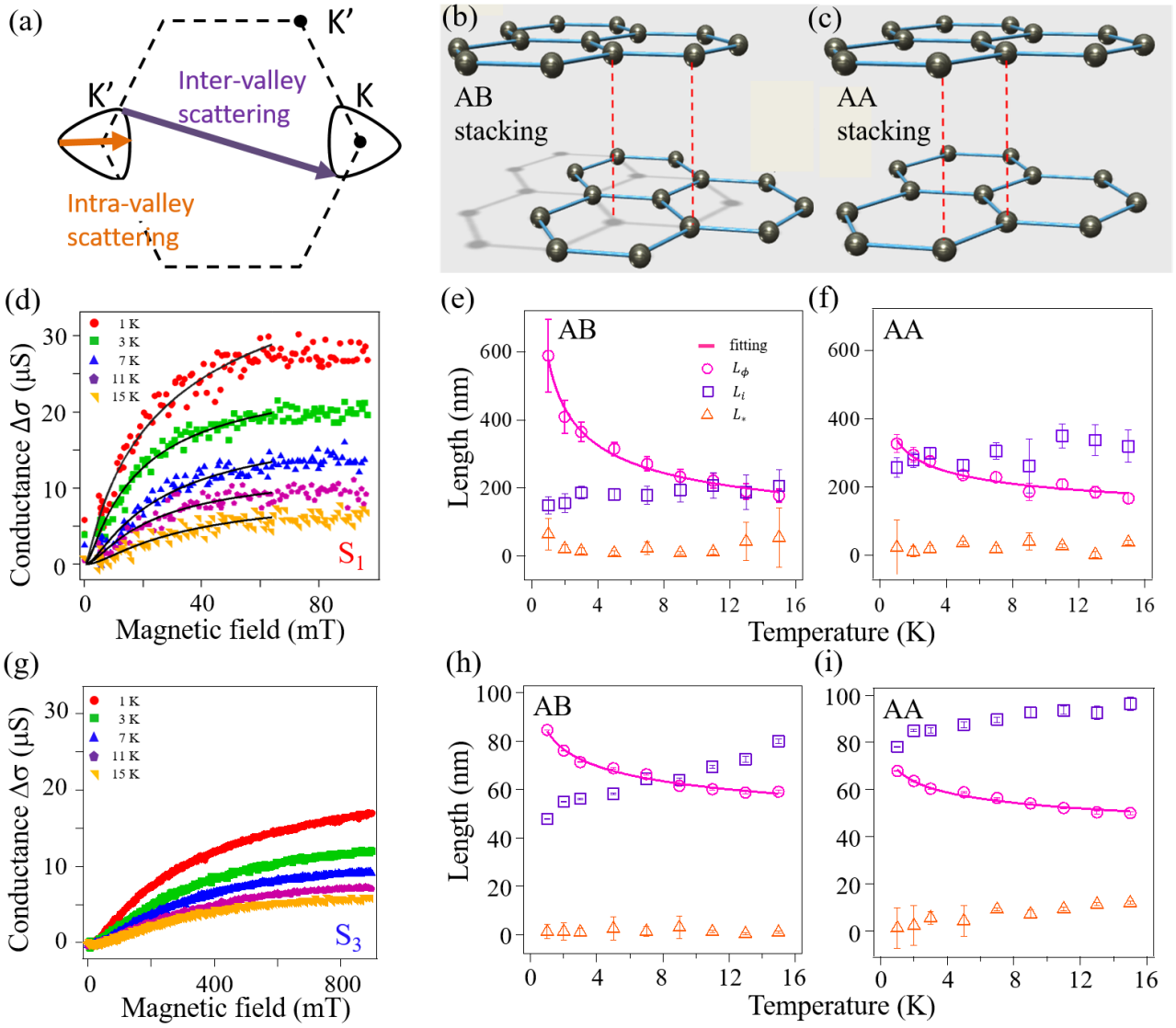


**Figure 3.** (a) Schematic view of inter- and intra-valley scattering paths on the Fermi surfaces in bilayer graphene. (b) and (c) AB and AA stacking sequence in bilayer graphene. (d) Magnetic field dependence of conductance at various temperatures for $S_1$. Black solid lines are fitting curves with equation (1). (e) and (f) Temperature dependences of the scattering lengths in $S_1$ which were derived by equations (1) and (2), respectively, i.e. the phase breaking scattering ($L_\phi$), the inter-valley scattering ($L_i$), and the intra-valley scattering ($L_*$) in $S_1$. Solid curve is a fitting with $L_\phi \propto T^{-P/2}$. (g) Magnetic field dependences of conductance at various temperatures for $S_3$. (h) and (i) Temperature dependences of the scattering lengths in $S_3$ which were derived by equations (1) and (2), respectively.

Next, we discuss the detail of transport properties in pristine bilayer graphene on SiC(0 0 0 1) substrate. In table 1, we compare the present results derived by equation (1) with previous reports [12, 13]. $\tau_{\phi,\mathrm{i},*}$ of graphene grown on SiC (two right columns) are smaller than those of exfoliated graphene (two left columns). Here, we discuss the relationship between the scattering time of carriers and its mechanism. First, we focus on $\tau_*$ for the intra-valley scattering in which the scattering occurs within each valley (figure 3(a)). In all cases in table 1, $\tau_*$ is much smaller than $\tau_\phi$ and $\tau_\mathrm{i}$, meaning that the intra-valley scattering occurs most frequently. This type of scattering with smaller changes in momentum can be induced by weaker scattering potentials compared with the inter-valley scattering. For the case of monolayer graphene grown on SiC, it is reported [13] that the intra-valley scattering can be induced by donors in the SiC substrate. Actually, the SiC wafer used as a substrate in our study has a high nitrogen dopant density of ~$1 \times 10^{18}$–$1 \times 10^{19}$ cm$^{-3}$. The Thomas–Fermi screening length is estimated to be 0.25–0.37 nm by taking into account the carrier density of degenerate semiconductor substrate [36]. The dopant density on the surface and the average distance between the nearest dopants in our SiC was estimated to be ~$3.7 \times 10^{10}$–$2.5 \times 10^{11}$ cm$^{-2}$ and 11–29 nm, respectively. As shown in figure 3(e), the intra-valley scattering length $L_*$ (which is theoretically independent of temperature) is 10–64 nm, which is comparable to the distance between the dopants on the SiC surface. Therefore, as one of the possible explanations, we infer that the nitrogen dopants in SiC substrate act as the main scatterers for the intra-valley scattering.

Then, let us discuss the inter-valley scattering time $\tau_\mathrm{i}$ of (monolayer and bilayer) graphene grown on SiC. In our case, it is much smaller than that of exfoliated graphene [12]. This

**Table 1.** Comparison of scattering times, $\tau_\varphi$, $\tau_i$ and $\tau_*$ at 3 K, among monolayer and bilayer graphene prepared by exfoliation or on SiC substrate.

| | Monolayer (exfoliated) [12] | Bilayer (exfoliated) [12] | Monolayer (SiC) [13] | Bilayer (SiC) (present study) |
|---|---|---|---|---|
| Carrier density ($10^{12}$ cm$^{-2}$) | 1.5 | 1.5 | 0.4 | 5.8 |
| $\tau_\varphi$ (ps) | 12 | 34 | 5.3 | 2.1 |
| $\tau_i$ (ps) | 18 | 47 | 1.0 | 0.55 |
| $\tau_*$ (ps) | 0.08 | 3 | 0.01 | 0.004 |

means that graphene grown on SiC has more defects than the exfoliated graphene. Such defects may produce strong potentials enough to induce the inter-valley scattering [12].

On the other aspect about the intra-valley scattering and inter-valley scattering, we also need to consider the carrier density in each sample because scattering events are proportional to the carrier density in accordance with Fermi's golden rule [37]. In table 1, bilayer graphene on SiC naturally has the carrier doping due to the charge transfer from the buffer layer, which is larger than that of the exfoliated graphene. This relation can explain that the intra and inter-valley scattering times of bilayer graphene on SiC are smaller in table 1.

Finally, we comment on the stacking structure of $S_3$ by comparing with *ex situ* measurements of transport of pristine bilayer graphene and Li-desorbed bilayer graphene under high magnetic field [38]. Our previous Shubnikov–de Haas (SdH) study has revealed that the Berry phase is nearly $\pi$ indicative of the AA stacking after desorbing intercalated Li atoms, while pristine bilayer graphene has nearly $2\pi$-Berry phase. This is not fully consistent with the present study in which the W(A)L analysis shows that the Berry phase of Li-desorbed bilayer graphene is neither $\pi$ nor $2\pi$, suggesting a mixture of several different stacking structures of AB, AA, and twisted stacking structures [39]. The SdH oscillations are in general more contributed by domains having higher carrier mobility and lower carrier density, while the W(A)L phenomena show a averaged property of all domains. Such a difference should be considered when interpreting the experimental results with different methods. It would be necessary to clarify the microscopic structure by future experiments.

## 4. Summary

We performed *in situ* electrical transport measurements for pristine bilayer graphene grown on SiC(0 0 0 1), Li-intercalated bilayer graphene, and that after desorbing the intercalated Li atoms. In all the three samples, we observed the increase of conductance at low temperatures upon applying the surface-normal magnetic field, which indicates the WL of carriers. By analyzing the data with the extended HLN equation, we have revealed the followings; (i) the magnetoconductance of pristine bilayer graphene is explained well by the AB stacking model, (ii) the phase breaking scattering is dominantly caused by the electron–electron scattering in a low temperature region (<15 K), (iii) dopants in the SiC substrate may cause a frequent intra-valley scattering in pristine bilayer graphene, and (iv) the Li-intercalation/desorption process produces additional scatterers and modifies the stacking structure. To investigate the irreversible structural change upon Li-treatments, further studies with a high spatial resolution such as scanning tunneling microscope are desired.

## Acknowledgments

This work was supported by JSPS KAKENHI Grant Numbers JP16H02108, JP16H00983, JP15H05854, JP25110010, JP15H02105, JP25107003, JP15K17464 and the Program for Key Interdisciplinary Research, Tohoku University.

## ORCID iDs

Y Endo https://orcid.org/0000-0003-2100-7722
R Akiyama https://orcid.org/0000-0003-3875-9509

## References

[1] Novoselov K S, Geim A K, Morozov S V, Jiang D, Zhang Y, Dubonos S V, Grigorieva I V and Firsov A A 2004 Electric field effect in atomically thin carbon films *Science* **306** 666–9
[2] Novoselov K S, Geim A K, Morozov S V, Jiang D, Katsnelson M I, Dubonos S V and Firsov A A 2005 Two-dimensional gas of massless Dirac fermions in graphene *Nature* **438** 197–200
[3] Novoselov K S, jiang Z, Zhang Y, Morozov S V, Stormer H L, Zeitler U, Maan J C, Boebinger G S, Kim P and Geim A K 2007 Room-temperature quantum Hall effect in graphene *Science* **315** 1379
[4] Bergmann G 1982 Influence of spin–orbit coupling on weak localization *Phys. Rev. Lett.* **48** 1046
[5] Bishop D J, Dynes R C and Tsui D C 1982 Magnetoresistance in Si metal-oxide-semiconductor field-effect transistors: evidence of weak localization and correlation *Phys. Rev.* B **26** 773
[6] Tikhonenko F V, Horsell D W, Gorbachev R V and Savchenko A K 2008 Weak localization in graphene flakes *Phys. Rev. Lett.* **100** 056802
[7] Chen Y-F, Bae M-H, Chialvo C, Dirks T, Bezryadin A and Mason N 2010 Magnetoresistance in single-layer graphene: weak localization and universal conductance fluctuation studies *J. Phys.: Condens. Matter* **22** 205301
[8] Di X, Chang M-C and Niu Q 2010 Berry phase effects on electronic properties *Rev. Mod. Phys.* **82** 1959–2007
[9] Kechedzhi K, McCann E, Fal'ko V I, Suzuura H, Ando T and Altshuler B L 2007 Weak localization in monolayer and bilayer graphene *Eur. Phys. J. Spec. Top.* **148** 39

[10] McCann E, Kechedzhi K, Fal'ko V I, Suzuura H, Ando T and Altshuler B L 2006 Weak-localization magnetoresistance and valley symmetry in graphene *Phys. Rev. Lett.* **97** 146805
[11] Kechedzhi K, Fal'ko V I, McCann E and Altshuler B L 2007 Influence of trigonal warping on interference effects in bilayer graphene *Phys. Rev. Lett.* **98** 176806
[12] Horsell D W, Tikhonenko F V, Gorbachev R V and Savchenko A K 2008 Weak localization in monolayer and bilayer graphene *Phil. Trans. R. Soc.* A **366** 245
[13] Lara-Avila S, Tzalenchuk A, Kubatkin S, Yakimova R, Janssen T J B M, Cedergren K, Bergsten T and Fal'ko V 2011 Disordered Fermi liquid in epitaxial graphene from quantum transport measurements *Phys. Rev. Lett.* **107** 166602
[14] Ichinokura S, Sugawara K, Takayama A, Takahashi T and Hasegawa S 2016 Superconducting calcium-intercalated bilayer graphene *ACS Nano* **10** 2761
[15] Margine E R, Lambert H and Giustino F 2016 Electron–phonon interaction and pairing mechanism in superconducting Ca-intercalated bilayer graphene *Sci. Rep.* **6** 21414
[16] Dresselhaus M S and Dresselhaus G 2002 Intercalation compounds of graphite *Adv. Phys.* **51** 1–186
[17] Sugawara K, Kanetani K, Sato T and Takahashi T 2011 Fabrication of Li-intercalated bilayer graphene *AIP Adv.* **1** 022103
[18] Kühne M, Paolucci F, Popovic J, Ostrovsky P M, Maier J and Smet J H 2017 Ultrafast lithium diffusion in bilayer graphene *Nat. Nanotechnol.* **12** 895–901
[19] Yamada M, Hirahara T, Hobara R, Hasegawa S, Mizuno H, Miyatake Y and Nagamura T 2012 Surface electrical conductivity measurement system with micro-four-point probes at sub-Kelvin temperature under high magnetic field in ultrahigh vacuum *J. Surf. Sci. Nanotechnol.* **10** 400–5
[20] van der Pauw L J 1958 A method of measuring specific resistivity and Hall effect of discs of arbitrary shape *Philips Tech. Rev.* **20** 220
[21] Rymaszewski R 1969 Relationship between the correction factor of the four-point probe value and the selection of potential and current electrodes *J. Phys.* E **2** 170
[22] Petersen D H, Lin R, Hansen T M, Rosseel E, Vandervorst W, Markvardsen C, Kjær D and Nielsen P F 2008 Comparative study of size dependent four-point probe sheet resistance measurement on laser annealed ultra-shallow junctions *J. Vac. Sci. Technol.* B **26** 362
[23] Virojanadara C, Zakharov A A, Watcharinyanon S, Yakimova R and Johansson L I 2010 A low-energy electron microscopy and x-ray photo-emission electron microscopy study of Li intercalated into graphene on SiC(0 0 0 1) *New J. Phys.* **12** 125015
[24] Hikami S, Larkin A I and Nagaoka Y 1980 Spin–orbit interaction and magnetoresistance in the two dimensional random system *Prog. Theor. Phys.* **63** 707
[25] Altshuler B L, Aronov A G and Lee P A 1980 Interaction effects in disordered fermi systems in two dimensions *Phys. Rev. Lett.* **44** 19
[26] Abrahams E, Anderson P W, Lee P A and Ramakrishnan T V 1981 Quasiparticle lifetime in disordered two-dimensional metals *Phys. Rev.* B **24** 12
[27] Gorbachev R V, Tikhonenko F V, Mayorov A S, Horsell D W and Savchenko A K 2007 Weak localization in bilayer graphene *Phys. Rev. Lett.* **98** 176805
[28] Wu X, Li X, Song Z, Berger C and de Heer W A 2007 Weak antilocalization in epitaxial graphene: evidence for chiral electrons *Phys. Rev. Lett.* **98** 136801
[29] Hsu Y F and Guo G Y 2010 Anomalous integer quantum Hall effect in AA-stacked bilayer graphene *Phys. Rev.* B **82** 165404
[30] Tabert C J and Nicol E J 2012 Dynamical conductivity of AA-stacked bilayer graphene *Phys. Rev.* B **86** 075439
[31] Abrahams E, Anderson P W, Licciardello D C and Ramakrishnan T V 1979 Scaling theory of localization: absence of quantum diffusion in two dimensions *Phys. Rev. Lett.* **42** 673
[32] Lee P A and Ramakrishnan T V 1985 Disordered electronic systems *Rev. Mod. Phys.* **57** 287
[33] Aitani M, Hirahara T, Ichinokura S, Hanaduka M, Shin D and Hasegawa S 2014 *In situ* magnetotransport measurements in ultrathin Bi films: evidence for surface-bulk coherent transport *Phys. Rev. Lett.* **113** 206802
[34] Mostaani E and Drummond N D 2015 Quantum Monte Carlo calculation of the binding energy of bilayer graphene *Phys. Rev. Lett.* **115** 115501
[35] Schmidt H, Rode J C, Smirnov D and Haug R J 2014 Superlattice structures in twisted bilayers of folded graphene *Nat. Commun.* **5** 5742
[36] Thomas L H 1927 The calculation of atomic fields *Proc. Camb. Phil. Soc.* **23** 542
[37] Jena D 2004 Charge transport in semiconductors *Advanced Semiconductor Physics* EE 698D
[38] Akiyama R, Takano Y, Endo Y, Ichinokura S, Nakanishi R and Hasegawa S 2017 Berry phase shift from $2\pi$ to $\pi$ in bilayer graphene by Li-intercalation and sequential desorption *Appl. Phys. Lett.* **110** 233106
[39] Rode J C, Smirnov D, Schmidt H and Haug R J 2016 Berry phase transition in twisted bilayer graphene *2D Mater.* **3** 035005